Definition of Redox Centers in Reactions of Lithium-Intercalation in Li₃RuO₄ Polymorphs

Haifeng Li,[†] Srinivasan Ramakrishnan,[‡] John W. Freeland,[§] Bryan D. McCloskey,[‡] Jordi Cabana*,[†]

[†]Department of Chemistry, University of Illinois at Chicago, Chicago, Illinois 60607, United States

[‡]Department of Chemical and Biomolecular Engineering, University of California, Berkeley, California 94720, United States

§Advanced Photon Source, Argonne National Laboratory, Lemont, Illinois 60439, United States

*corresponding author: <u>jcabana@uic.edu</u>

Abstract

Cathodes based on layered LiMO₂ are the limiting components in the path toward Li-ion batteries with energy densities suitable for electric vehicles. Introducing an over-stoichiometry of Li increases storage capacity beyond a conventional mechanism of formal transition metal redox. Yet the role and fate of the oxide ligands in such intriguing additional capacity remain unclear. This reactivity was predicted in Li₃RuO₄, making it a valuable model system. A comprehensive analysis of the redox activity of both Ru and O under different electrochemical conditions was carried out, and the effect of Li/Ru ordering was evaluated. Li₃RuO₄ displays highly reversible Li intercalation to Li₄RuO₄ below 2.5 V vs. Li⁺/Li⁰, with conventional reactivity through the formal Ru⁵⁺-Ru⁴⁺ couple. In turn, it can also undergo anodic Li extraction at 3.9 V, which involves of O states to a much greater extent than Ru. This reaction competes with side processes such as electrolyte decomposition and, to a much lesser extent, oxygen loss. Although the associated

capacity is reversible, re-intercalation unlocks a different, conventional pathway also involving the formal Ru⁵⁺-Ru⁴⁺ couple despite operating above 2.5 V, leading to chemical hysteresis. This new pathway is both chemically and electrochemically reversible in subsequent cycles. This work exemplifies both the challenge of stabilizing highly depleted O states, even with 4*d* metals, and the ability of solids to access the same redox couple at two very different potential windows depending on the underlying structural changes. It highlights the importance of properly defining the covalency of oxides when defining charge compensation in view of the design of materials with high capacity for Li storage.

1. Introduction

Rechargeable Li-ion batteries have conquered the market of electronic devices, enabling the realization of the wireless revolution in our society over the past two decades, and they are touted in the pivot to a sustainable and green economy with electrified vehicles.^{1,2} Moreover, they have the potential for grid applications that could boost the use of renewable sources on a large scale.³ For such an attractive future to emerge, high-capacity materials for the cathodes are vital to further increase the capability of batteries to store energy from today's levels.^{4,5,6} Currently, Li-ion batteries are limited by the ability of transition metal oxides to reversibly intercalate Li without electrochemical degradation. In practical applications, a maximum of 0.6-0.7 mol electrons per mol of transition metal, for a specific capacity below 200 mAhg⁻¹, can be cycled in a stable fashion, thus limiting storage below their theoretical value.⁷ Therefore, new battery chemistries that can effectively bypass this limitation are the focus of intensive research.

In comparison with the first-generation cathode, layered rock-salt-type LiCoO₂,⁸ the partial substitution of Co by Ni and Mn greatly promoted storage, potentially crossing the threshold of

200 mAhg⁻¹ while remaining durable, resulting into the widely commercialized positive materials $Li(Co_{I-x-y}Ni_xMn_y)O_2$ (NMC). ^{9,10} However, this is still far from the capacity of the commercial graphite anodes (350 mAhg⁻¹). To further enhance the energy density, recently, materials have been designed through an over-stoichiometry of Li to partially replace the transition metals in the corresponding layer to form $Li[Li_xTM_{1-x}]O_2$ (TM: transition metal), which have led to capacities up to 260 mAhg⁻¹ in small-scale prototypes. ¹¹⁻¹⁵ These oxides transcend traditional battery mechanisms by tapping the formal redox activity of oxide ligands as well as the transition metal centers. However, the long-term durability of these materials has been so far compromised precisely by this extensive reactivity, which results in loss of oxygen form the lattice, detrimental structural reorganization and irreversible interfacial phenomena, leading to low energy efficiency and resilience.

The promise of the concept has spurred intense interest into establishing the fundamental ability of oxides to undergo ligand-centered redox transitions, by exploring the role of transition metal bonding and atomic arrangements. Using Li₂Ru_{1-y}Sn_yO₂ as a model system, Sathiya *et al.* first proposed the existence of a lattice O²⁻/O⁻ redox process, separate from the formal oxidation of Ru.¹⁶ Subsequent investigations of cation disordered rock-salt structures like Li_{1.2}Ni_{1/3}Ti_{1/3}Mo_{2/15}O₂,¹⁷ Li_{1.25}Nb_{0.25}Mn_{0.5}O₂,¹⁸ Li_{1.3}Mn_{0.4}Nb_{0.3}O₂,^{19, 20} Li₄Mn₂O₅,²¹ and three-dimensionally ordered rock-salt β-Li₂IrO₃²² have claimed to support this ligand-centered activity, suggesting that pathways exist toward materials with practical use in a realistic device. Meanwhile, computational studied have served to rationalize the underlying mechanisms of Li-rich oxides. Seo *et al.* revealed the substantial contribution of Li-O-Li linear clusters in Li[Li_xTM_{1-x}]O₂, due to the presence of Li in both types of layers, to the advent of labile non-bonding O 2*p* bands near the Fermi level, which can be tapped in a redox process involving only O.²³ In parallel, the metal-

driven redox coupling mechanism was proposed by Saubanere *et al.*, unveiling the crucial role of the covalency between O and transition metals in stabilizing the O holes generated in an anionic redox process.²⁴ Subsequently, Xie *at al.* showed that the number of pure lone O 2*p* states relies on the O/TM ratio, which is proportional to the non-bonding O 2*p* states at the Fermi level that could induce additional capacities in Li-rich cathode materials.²⁵ These huge capacities were subsequently realized in layered Li₃IrO₄.²⁶ Overall, these pioneering works have built a sound scientific foundation for the design of high-capacity Li-rich positive materials by modifying the structure or tuning the O/TM ratio through control of composition. Yet the exact role of anions, especially in terms of the existence and reversibility of activity only centered at the oxide ligands, remains to be established.

Following the Li₃*TM*O₄ (or Li[Li_{0.5}*TM*_{0.5}]O₂) family, Yabuuchi *et al.* demonstrated that Li₃NbO₄, with an ordered rock-salt structure, is electrochemically inactive due to the absence of electrons in the conduction band.¹⁹ Jacquet *et al.* reported ordered, layered structures showing a variety of interlayer arrangments can be generated by substituting Nb with Ru.²⁷ They revealed that it was possible to both remove Li to formally form Li_{3-x}Ru_yNb_{1-y}O₄, with x largely correlating with *y*, and insert Li to form Li₄Ru_yNb_{1-y}O₄. Subsequently, they explored the intercalation chemistry of Li₃Ru_yIr_{1-y}O₄.²⁸ Focusing on Li₃RuO₄, the two articles probed the extraction of the charge equivalent to full delithiation ("RuO₄"), and reported a significant tendency toward dissolution of Ru in the form of oxo-complexes. However, the charge compensation mechanism was not completely elucidated, so it is unclear whether ligand-centered reactivity was realized. Furthermore, the role of structural ordering was not evaluated, yet both layered and disordered rock-salt forms of Li₃RuO₄ are known.^{29,30}

In this study, the origin of the electrochemical properties of the two rock-salt polymorphs of

Li₃RuO₄, disordered and layered, was ascertained. The structures are composed of arrangements of LiO₆ and RuO₆ edge-sharing octahedra with different distributions. Both polymorphs show rich electrochemistry along a very broad compositional space, from nominally Li₂RuO₄ to Li₄RuO₄. To fully understand this chemistry, with the goal of defining the redox centers underpinning the reaction, the different states were characterized with a combination of probes of crystal structure and the electronic structure at both Ru and O. The results revealed that both conventional metal-centered intercalation reactions and ligand-centered process are possible in this compound. Their reversibility and the broad implications for the design of materials with high capacity for charge storage are established.

2. Results and Discussion

2.1 Structural Characterization of Li₃RuO₄

Li₃RuO₄ crystallizes in a rock-salt structure, but the degree of Li/Ru ordering within the octahedral sites varies with increasing temperature.^{29, 31} Joint Rietveld refinement of SXRD and NPD agreed with reports in the literature and confirmed the purity of the synthesized materials. At 650°C, the oxide crystallized in a simple rock-salt structure with a random arrangement of Li and Ru (D-Li₃RuO₄, Figures S1a and S2a, and Table S1a). A broad hump that could not be indexed by this structure was found centered at Q ~1.3 Å⁻¹, which suggested short-range ordering of Li/Ru. The oxide made at 900°C showed Li/Ru ordering into alternating Li-only and Li/Ru layers within the rock-salt framework (O-Li₃RuO₄, Figures S1b and S2b, and Table S1b).^{31, 32} Li and Ru are also ordered within [Li_{1/2}Ru_{1/2}]O₂ layers forming zig-zag chains of [RuO₆] and [LiO₆] octahedra (Figure S2b). The refinements did not improve with the introduction of Li vacancies or the partial occupancy of Ru in Li sites described previously.²⁷ Ru adopts a slightly distorted environment

with pairs of Ru-O distances at 1.91, 1.98, and 2.05 Å (Figure S3 and Table S2), thus with Ru displaced from the octahedron center.³⁰ The coordination environment could not be evaluated for D-Li₃RuO₄ because of the Li and Ru disorder (Figure S3). The particles of both polymorphs were around 1 μm and displayed irregular morphologies (Figure S4).

2.2 Voltage cutoff window of 2.5-3.9 V

Potential-composition profiles were measured galvanostatically under two windows. Between 3.9 and 2.5 vs Li⁺Li⁰, the experiment was initiated upon oxidation of Li₃RuO₄, to explore the hypothetical reaction

$$Li_3RuO_4 \rightarrow Li_2RuO_4 + Li^+ + e^- \tag{1}$$

while minimizing effects from amorphization and transition metal dissolution at higher potential.²⁸ In turn, reduction was the first step between 1.5 and 2.5 V, for the hypothetical reaction:

$$Li_3RuO_4 + Li^+ + e^- \rightarrow Li_4RuO_4$$
 (2)

2.2.1 Electrochemical properties of Li₃RuO₄

Electrochemical activity of D-Li₃RuO₄: Starting from oxidation, the electrochemical cell with D-Li₃RuO₄ displayed a plateau with an average voltage of 3.8-3.85 V vs Li⁺/Li⁰ (Figure 1a), accumulating a capacity equivalent to the removal of just under 2 mol Li per mol compound. The corresponding derivative curve (Figure 1b) showed a sharp process centered at 3.8 and a small one at 3.84 V. Upon reduction, the slope of the potential-composition profile notably increased, leading to the absence of clear plateaus. There was a broad peak at 3.6 V in the derivative curve with a shoulder at 3.4 V. The total associated capacity was equivalent to 1.1 mol Li per mol compound. Upon subsequent cycling, the electrochemical profiles continued to wash out, with most activity

occurring below 3.8 V, and the total capacity declined (Figure S5).

Electrochemical activity of O-Li₃RuO₄: Turning to O-Li₃RuO₄, the profile showed a flat plateau at around 3.87 V vs Li⁺/Li⁰, corresponding to the removal of 0.5 mol Li per mol compound at 3.9 V (Figure 1c), less than D-Li₃RuO₄. On the subsequent reduction, the plateau in the voltagecomposition was centered at 3.67 V, followed by a sharp decrease in the voltage, denoting again a significant hysteresis. The coulombic efficiency in this first cycle was also low, only ~0.3 mol Li being recovered. The profiles significantly evolved with cycling. First, the anodic step above 3.85 V gave way to a new process at 3.75 V, which was accompanied by a cathodic process at 3.7 V and a notable reduction in hysteresis. Upon further cycling, the anodic profile evolved to consist of a long sloping feature up to 3.75 V, followed by a rather flat plateau at 3.8 V. This profile was highly reversible upon reduction, with the plateau centered at 3.7 V. This evolution was complete around cycle 20, and it was accompanied by a dramatic increase in the amount of charge equivalent of 1 mol Li per mol O-Li₃RuO₄. The capacity was almost 100% reversible upon cycling, and it remained stable for several subsequent cycles (Figure S6). Overall, the evolution in the electrochemical profiles suggests that the compound is activated by cycling, with a notable complexity in the associated redox reaction.

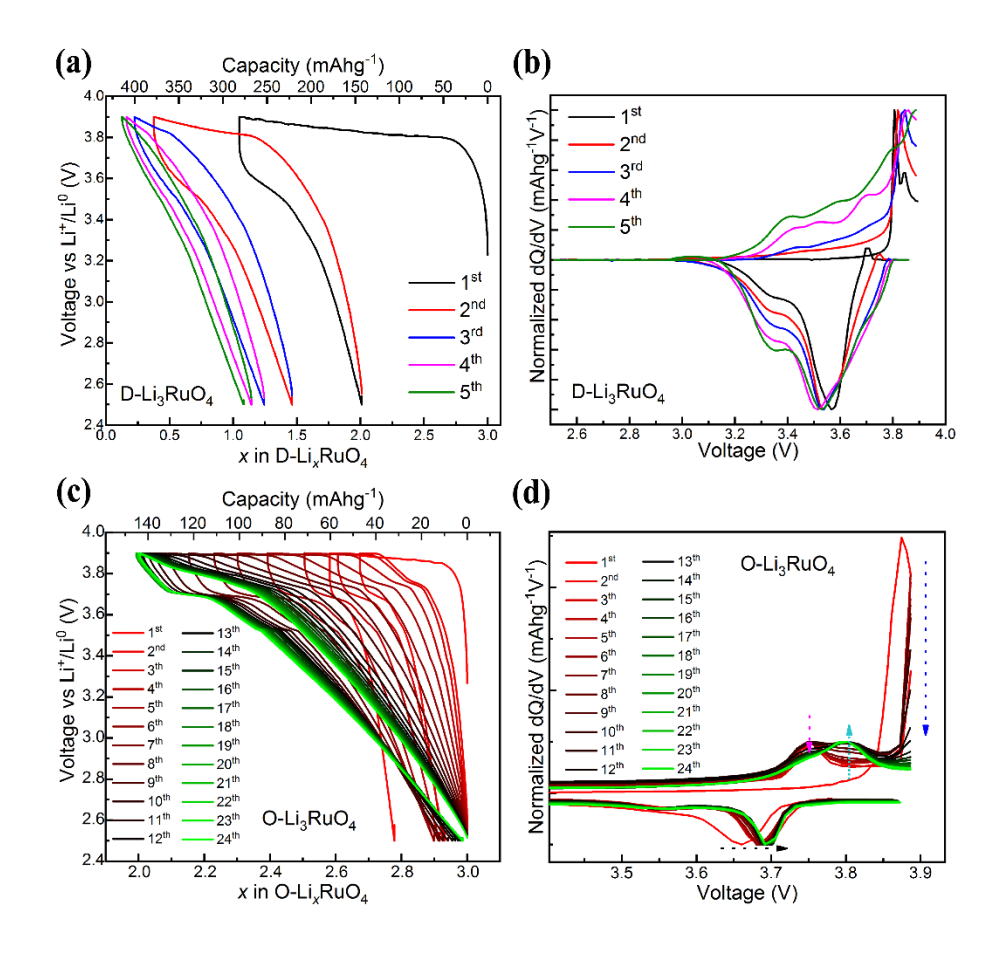


Figure 1. Voltage-composition profiles of (a) D-Li₃RuO₄ and (c) O-Li₃RuO₄ between 2.5-3.9 V; differential capacity analysis (dQ/dV) of (b) D-Li₃RuO₄ and (d) O-Li₃RuO₄. The profiles in (c) were re-scaled back to x=3 (0 mAhg⁻¹) for clarity, with Figure S6 showing the data without shifting.

2.2.2 Structural evolution of Li₃RuO₄

 $D\text{-}Li_3RuO_4$ between 2.5 and 3.9 V: Figure 2 presents the variation of SXRD patterns of D-Li₃RuO₄ at the end points in the first cycle collected *operando* (Figure S7). There was a general decrease in the peak intensity and increase in the peak width, indicating a significant loss of crystallinity. It was accompanied by a shift to lower angle in their position, indicating an increase in unit cell volume, which was unexpected from a conventional reaction of deintercalation of Li⁺. In addition, the delithiation led to the appearance of three new peaks located at Q (2 θ angle) of 2.5

Å⁻¹ (5.9°), 2.5 Å⁻¹ (8.3°) and 2.5 Å⁻¹ (10.2°) as denoted by stars (Figure 2), accompanied by a tail at low angles in the intense reflection at 3.3 Å⁻¹, possibly indicating growth of either a newly formed phase or a lowering of the symmetry of the disordered rock-salt framework. Upon subsequent reduction to 2.5 V, the broad low-angle peak experienced no obvious changes while the other peaks returned to the position of the pristine state with a partial recovery of intensity, and the new peaks induced by oxidation almost vanished. Due to the limited number of Bragg reflections and the broadening of the patterns, it was not possible to assign the newly formed peaks to a specific phase or distortion. Therefore, the cell parameters were obtained by the Pawley refinement based on disordered rock-salt with a cubic space group Fm3m without including the low-Q broad peak, as shown in Table 1 and Figure S8. The underlying lattice volume of the fully delithiated state increased by 1.6% compared with that of the pristine state and, while it diminished after the following reduction, it remained larger than the pristine state by 0.5%.

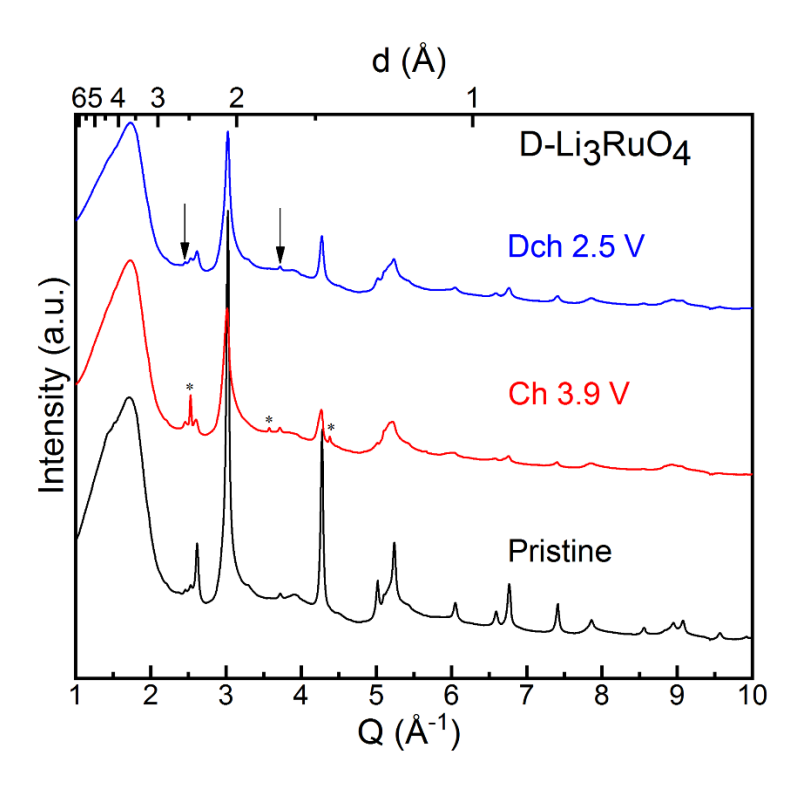


Figure 2. SXRD patterns of D-Li₃RuO₄ at selected points during the first cycle within a potential range of 2.5-3.9 V, collected *operando*. The complete evolution of the data is found in Figure S7. The black arrows denote Bragg reflections that could not be indexed by the parent rock-salt lattice, which also did not change with cycling. The stars represent the newly formed peaks concurrent with Li (de)intercalation.

O-Li₃RuO₄ between 2.5 and 3.9 V: The ex situ XRD patterns of O-Li₃RuO₄ after the 1st oxidation-reduction cycle showed little change in the position and width of Bragg reflections, with, at most, minor changes in intensity (Figures 3a, S9 and S10a, and Table 1). The marginal variations are consistent with the small capacity observed. Samples were also harvested at cycles where the highest capacity was observed (Figure 3b). The corresponding XRD pattern upon oxidation showed significantly different peak positions compared to both pristine and the first charge, with observable broadening. Subsequent reduction then brought about a narrowing and shift of the peaks to the original positions. According to Pawley fits of the data using a P2/a space group (Table 1 and Figure S10b), the unit cell volume expanded by 5.1% relative to the pristine state upon charging, whereas it shrunk back upon discharge, being 0.2% smaller than the pristine state. It must be noted that the fit of the pattern of the charged state failed to completely account for some of the complex peak shapes at low Q. This effect suggests a subtle distortion of the structure.

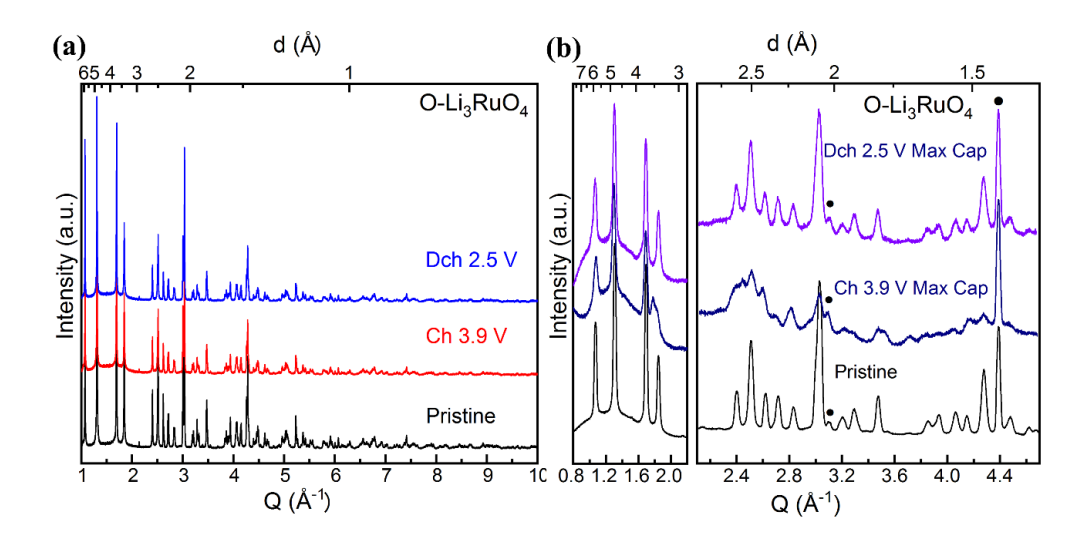


Figure 3. (a) Ex situ SXRD patterns of ordered Li₃RuO₄ after the first cycling; (b) Ex situ Laboratory XRD patterns when the capacity reached maximum. The black dots represent the Bragg reflections from Al foil. "Max Cap" in (b) is the abbreviation of "Maximum Capacity".

Table 1. Calculated Unit Cell Parameters via Pawley refinement of the data in Figure 3 and 4.

		D-Li ₃	RuO ₄					
State		a = b = c (Å)		Volume (Å ³)				
Pristine		4.14929	71.436					
Ch 3.9 V		4.17061	72.543					
Dch 2.5 V		4.15651	71.810					
O-Li ₃ RuO ₄								
State	a (Å)	b (Å)	c (Å)	β (°)	Volume (Å ³)			
Pristine	5.08809	5.86792	5.12213	110.154	143.566			
Ch 3.9 V	5.08869	5.86786	5.12070	110.128	143.565			
Dch 2.5 V	5.08832	5.86845	5.11979	110.123	143.548			
Ch 3.9 V Max Cap	5.19202	5.96737	5.25034	111.963	150.863			

Dch 2.5 V 5.05296 5.89378 5.12716 110.264 143.241 Max Cap

2.2.3 Ex situ Ru K-edge XAS of Li₃RuO₄

Ex situ Ru K-edge X-ray absorption near edge structure (XANES) spectra were collected of D-and O-Li₃RuO₄ (Figures 4 and 5). The first derivative of the spectra was used to establish the position of the absorption edge, using the first inflection point above 22120 eV. The main absorption edge arises from the electric dipole-allowed transition from the 1s to 5p level, whilst the pre-edge arises from two primary transitions.³³ One is the electric quadrupole-allowed and dipole-forbidden $1s \rightarrow 4d$ transition. The probability of the electric quadrupole-allowed transitions is much lower compared with the dipole, leading to a much lower intensity in the pre-edge peak. However, an enhancement of its intensity can be induced by symmetry-breaking distortions of an octahedron that remove its inversion center, thus promoting mixing between 4d and 5p orbitals. The pre-edge peak generally had low intensity in the pristine spectra, indicating that the displacement of Ru off the center of the RuO6 octahedra was not sufficient to induce visible enhancement. The strong similarity in the spectra of the two polymorphs suggests similar local coordination environment of Ru (Figure S11). The oxidation state of Ru⁵⁺ was confirmed by comparing the rising edge and the first derivative curve of the Ru K-edge XANES spectra with $Ru^{4+}O_2$ (Figures 4a, 5a, and S11).

D-Li₃RuO₄ between 3.9 and 2.5 V: Upon oxidation of D-Li₃RuO₄ to 3.9 V, there was almost no energy shift of the rising edge compared with the pristine state (Figure 4a). However, there was an apparent growth of the pre-edge peak after oxidation (Figure 4b), as denoted by a small derivative peak at 22117 eV, and a decrease in the ratio between the whiteline peaks at 22138 and 22150 eV. This observation could be attributed to the distortion of the coordination environment

of Ru through enhanced hybridization between Ru 5p and 4d orbitals. Overall, the changes are consistent with the onset of a new Ru species reported by Jacquet et al. at similar potentials, on the way to complete nominal delithiation.²⁸ In contrast, there was a notable shift of ~1.9 eV of the absorption edge towards lower energy after the subsequent reduction process to 2.5 V. Indeed, the resulting spectrum largely overlapped with Ru⁴⁺O₂, hence unambiguously demonstrating the reduction of Ru and the existence of different chemical pathways upon oxidation and reduction in this first cycle. A pre-edge peak was no longer resolved, implying the recovery of a largely centrosymmetric coordination environment of Ru.

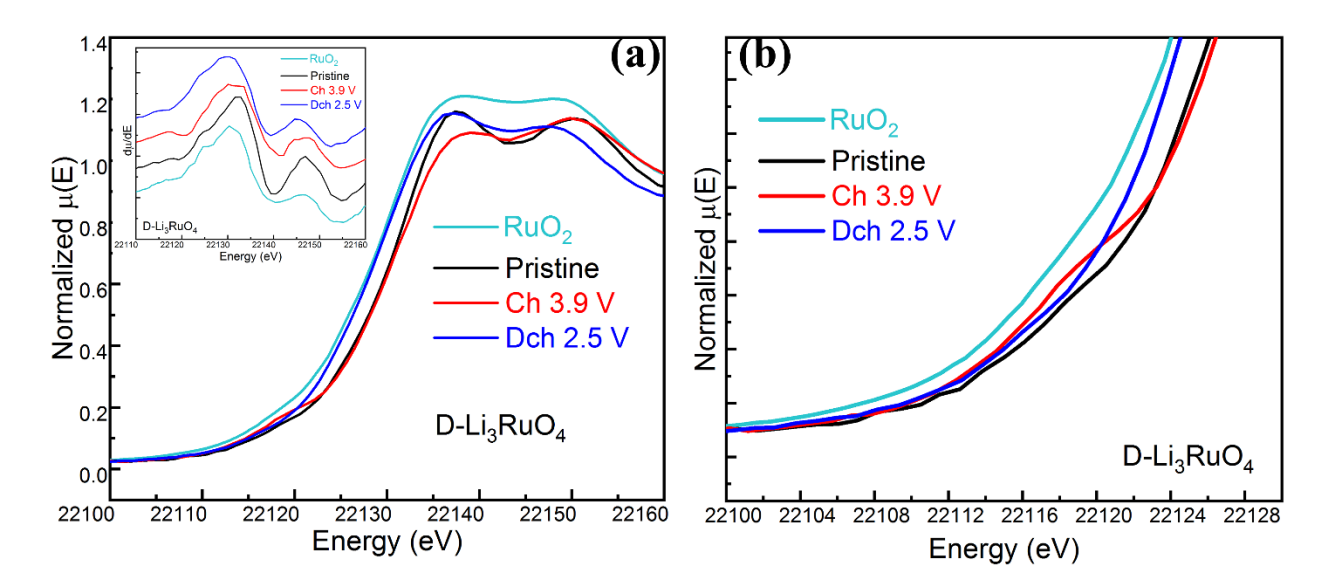


Figure 4. (a) *Ex situ* Ru K-edge XANES spectra of D-Li₃RuO₄ at different electrochemical states and (b) zoom of the pre-edge region. The inset in (a) presents the corresponding derivative curves, used to define the position of the absorption edge. RuO₂ was used as reference for Ru⁴⁺.

O-Li₃RuO₄ between 3.9 and 2.5 V: The Ru K-edge XANES spectrum of O-Li₃RuO₄ after initial oxidization to 3.9 V (Figure 5a) overlapped with the pristine state, with only a slight increase in the pre-edge intensity. The following reduction process to 2.5 V caused the rising edge to shift

toward lower energy by \sim 1.1 eV relative to the pristine state, close to the RuO₂ standard, with loss of any pre-edge features. When the electrochemical reactivity reached its maximum after multiple cycles (Figure 5a), the position of the rising absorption edge of the charged electrode still mostly overlapped with the pristine state (derivative peak in the inset of Figure 5a), but there was an increase in the intensity of the pre-edge peak (Figure 5b). This phenomenon is likely due to the redox-driven distortion in the symmetry of RuO₆. The subsequent reduction shifted the edge to lower energy by \sim 1.5 eV relative to the pristine state, close again to the Ru⁴⁺ state of RuO₂, with low pre-edge intensity, again suggesting RuO₆ centrosymmetry.

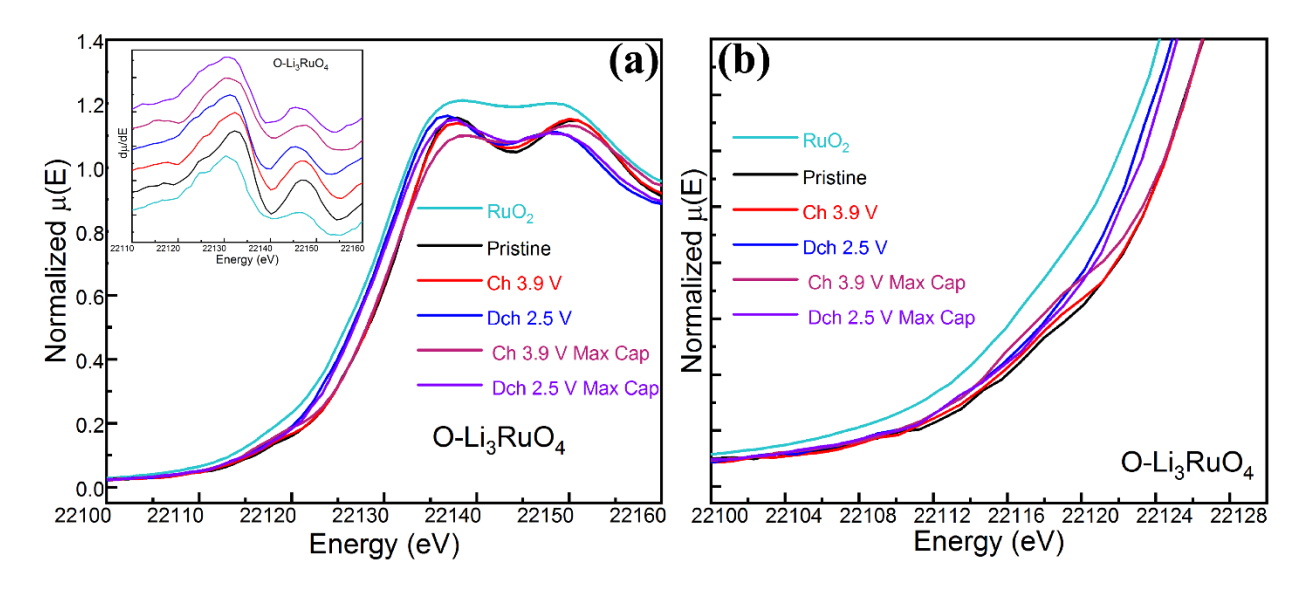


Figure 5. (a) *Ex situ* Ru K-edge XANES spectra of O-Li₃RuO₄ at different electrochemical states and (b) zoom of the pre-edge region. The inset in (a) presents the corresponding derivative curves, used to define the position of the absorption edge. RuO₂ was used as reference for Ru⁴⁺. "Max Cap" here denotes data at cycles with maximum capacity (see text).

2.2.4 Ex situ O K-edge XAS of Li₃RuO₄

General features of the pristine states. The O K-edge XAS probes dipole-allowed transition

from core O Is to empty O 2p states.³⁴ In general, the spectra of these transition metal compounds can be divided into two regions. The pre-edge, at ≤ 535 eV, represents the unoccupied states resulting from O 2p orbitals hybridized with Ru 4d orbitals, and the broad band above 535 eV corresponds to the excitation from O 1s orbital to empty states of O 2p orbitals mixed with the Ru 5s and 5p orbitals, followed by higher states and multiple scattering events of the ejected electrons. The position of the pre-edge peak is affected by the change in the net electron density of the ligand via donating charge to the surrounding metal ion, which affects the attraction of electrons by the effective nuclear charge Z_{eff}, the degree of d orbital splitting induced by the crystal field effect, and the overall d-manifold energy determined by the strength of the covalent Ru-O bonds.³⁵ The intensity of these peaks reflects both the number of unoccupied hybridized states and the contribution of O to their wavefunction.³⁶ Therefore, the measurements offer insight into the role of O states and any changes in covalency. Note that the XAS spectra were measured simultaneously under both TEY and TFY modes. The TEY mode with a probing depth around 10 nm provides the surface information, whereas TFY mode probes 100-nm into the electrode, offering insight into the interior of the material. It is worthy of notice that spectral intensities in this mode are distorted by the self-absorption of fluorescent photons by the material, so only qualitative trends between samples will be established.

The O K-edge XAS spectra of pristine D- and O-Li₃RuO₄ exhibit distinct pre-edge features centered at 528.4, 529.2, and 531.5 eV (Figure 6). There was also a prominent peak at 533.8 eV in both TEY and TFY spectra of D-Li₃RuO₄ (Figure S12), but it was only clearly visible in the TEY of O-Li₃RuO₄ (Figure S13). Since the O K-edge spectrum of Li₂CO₃ has a strong feature at similar energy,³⁷ the higher intensity in the surface-sensitive spectra suggests that it contributed as an impurity in the sample, which could not be detected by XRD (Figure S1). Electrochemical

decomposition of Li₂CO₃ usually occurs above 4.3 V.³⁸ Since a cutoff voltage of 3.9 V was used here, the peak arising from Li₂CO₃ largely remained after charging (Figure S12 and Figure S13), confirming that it was not significantly electroactive in these conditions. Due to the dominant role of Li₂CO₃ in the TEY spectra, analysis mainly focused on the TFY mode.

In accordance with crystal field theory, the envelope below 530 eV is assigned to the unoccupied states with contribution from Ru $4d_{xz}$, $4d_{yz}$, and $4d_{xy}$, whereas the broad signal centered at 531.5 eV is assigned to states hybridized with $4d_z^2$ and $4d_x^2^2$. The fine structure observed in the peaks, especially below 530 eV strongly suggests a lifting of the t_{2g}/e_g degeneracy in an ideal octahedral field, consistent with the distortion of the RuO₆ octahedra in the rock-salt framework, triggered by the off-center positioning of Ru. The high similarity in the pre-edge signals between D- and O-Li₃RuO₄ strongly suggests that the local distortion is similar in both structures. The qualitatively lower intensity in the $4d_{xz}/d_{yz}/d_{xy}$ compared to d_z^2/d_x^2 -y² signals reflects the d³ configuration of Ru(V).

 $D\text{-}Li_3RuO_4$ between 3.9 and 2.5 V: On oxidation of D-Li_3RuO_4 to 3.9 V, the main absorption threshold moved to higher energy by ~0.5 eV relative to the pristine state (Figures 6a and S14a), denoting variations in the O 1s energy level relative to the continuum due to an increase in Z_{eff}. The two peaks below 530 eV were reduced to one located at 529.9 eV with a diminished absorption intensity, while the broad peak centered at 531.5 eV in the pristine state moved to higher energy, around 532.3 eV, along with an increased intensity. The changes in the peak position and intensity of pre-edge part reflected the notable changes taking place in the hybridization of the O 2p-Ru 4d orbitals. Given that Ru states remained largely unchanged, according to Ru K-edge XANES, those changes should originate from a localized variation in the oxygen electronic changes concurrent with oxidation.

Upon subsequent reduction to 2.5 V, the onset position of the absorption edge experienced a lower-energy shift of ~0.6 eV in comparison with the oxidized state, but was slightly lower relative to the pristine state (Figures 6a and S14a). Both pre-edge peaks slightly shifted to lower energy, appearing at 529.4 and 532.2 eV, with a concurrent decrease in intensity by 25.0% and 14%, respectively, when compared with the oxidized state. The decrease in the intensity would be consistent with the reduction leading to electrons into previously unoccupied orbitals, in conjunction with the observed Ru⁵⁺/Ru⁴⁺ reduction in the Ru K-edge XANES.

O-Li₃RuO₄ between 3.9 and 2.5 V: The oxidation of O-Li₃RuO₄ crossing 3.9 V shifted the threshold of the absorption edge to higher energy relative to the pristine state (Figure 6b and S14b). There was an apparent increase in the intensity of the pre-edge region in comparison with the pristine state (Figure S14b), with very minor changes in shape and peak distribution. The subsequent reduction led to a low-energy shift of the absorption threshold, to a position lower than the pristine state. There was a loss of intensity of the pre-edge peaks below 530 eV, especially at the lowest energies, leaving a dominant peak at around 529.4 eV, with a small shoulder to the left. Above 530 eV, the position and shape of the broad pre-edge peak remained almost invariable, yet with an observable decrease in the intensity. Analogous with Ru K-edge XANES, the O K-edge XAS spectra were also recorded after multiple cycles when the electrochemical capacity reached its maximum. The trends observed in the first cycle were mirrored at this point, suggesting a reversible cycling between the same states after cycle 2, as the electrochemical curve evolved into a multi-step process.

Overall, the observed qualitative trends in the O K-edge spectra were the same in both polymorphs. The most salient observation is that reduced states upon cycling were systematically different from the initial spectrum for O-Li₃RuO₄, emphasizing the different pathways during the

first charge and subsequent redox cycling observed by Ru K-edge XANES.

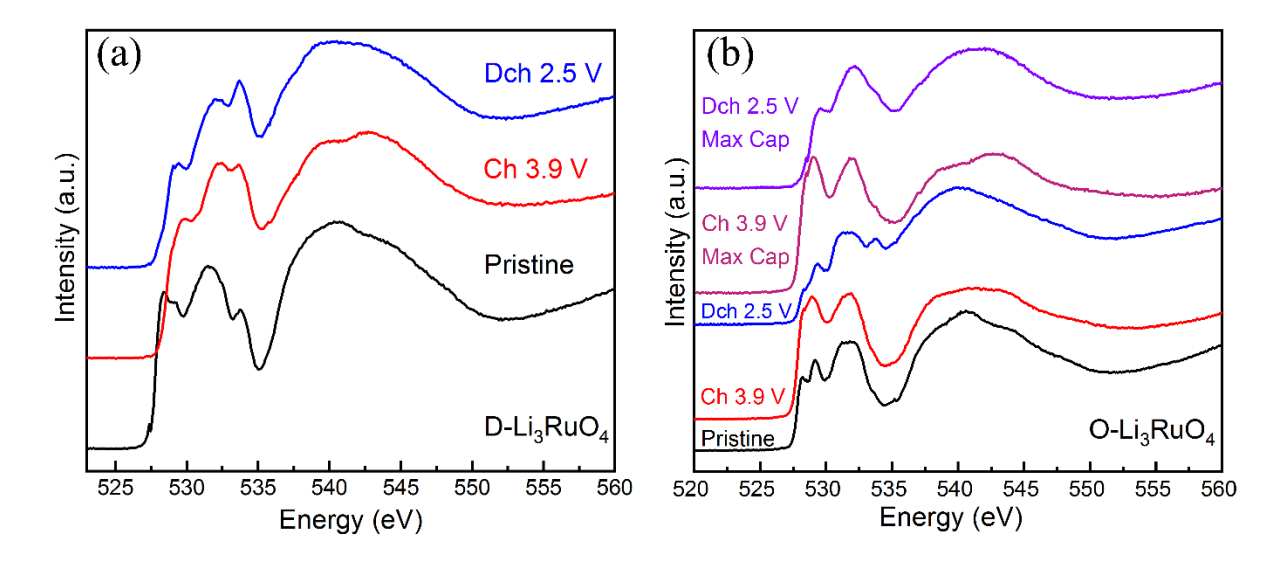


Figure 6. Ex situ O K-edge XAS spectra of (a) D- and (b) O-Li₃RuO₄ measured at different electrochemical states between 2.5-3.9 V. "Max Cap" in (b) is the abbreviation of "Maximum Capacity". The peak at ~533.8 eV is ascribed to the existence of Li₂CO₃ in both (a) and (b).

2.2.5 Operando analysis of gas evolution

A charge and discharge capacity of 205 mAh/g and 131 mAh/g, respectively, were obtained for D-Li₃RuO₄ during *operando* gas analysis using differential electrochemical mass spectrometry (DEMS, Figure 7), only slightly lower than the analogous values from coin cell testing. O₂ evolution, likely originating from the active cathode material, had an onset near the beginning of the long plateau region in the charge profile with a cumulative 0.42 μmol, whereas CO₂ evolution was slightly delayed, with an overall 1.9 μmol much larger than O₂ (Table S3). Since residual surface Li₂CO₃ decomposes to produce CO₂ above 4.3 V,^{39, 40} and based on the analysis of O K-edge XAS in TEY mode discussed above, we assign the CO₂ in Figure 7 primarily to electrolyte decomposition. The amount of O₂ evolved from the cathode (0.42 μmol) corresponds to 0.64% of

the lattice oxygen (5.9 mg has an equivalent of 64 μ mol O). Considering the electron stoichiometry of 4 e⁻/O₂, the total irreversible capacity brought about by the oxygen loss was ~8 mAh/g.

O-Li₃RuO₄ exhibited a voltage profile similar to the results in coin cells, with higher capacity during both charge (200.3 mAh/g) as well as discharge (69.1 mAh/g) in the first cycle, mainly derived from the high cutoff voltage of 4.0 V. Both O₂ and CO₂ started to appear simultaneously as the delithiation occurred, with a cumulative amount of 0.3 and 2.2 μmol, respectively, after the first cycle (Table S3). The total O₂ evolved corresponds to 0.40% of the lattice oxygen (7.0 mg has an equivalent of 76 μmol O), which corresponds to an irreversible capacity of ~5 mAh/g, lower than in D-Li₃RuO₄.

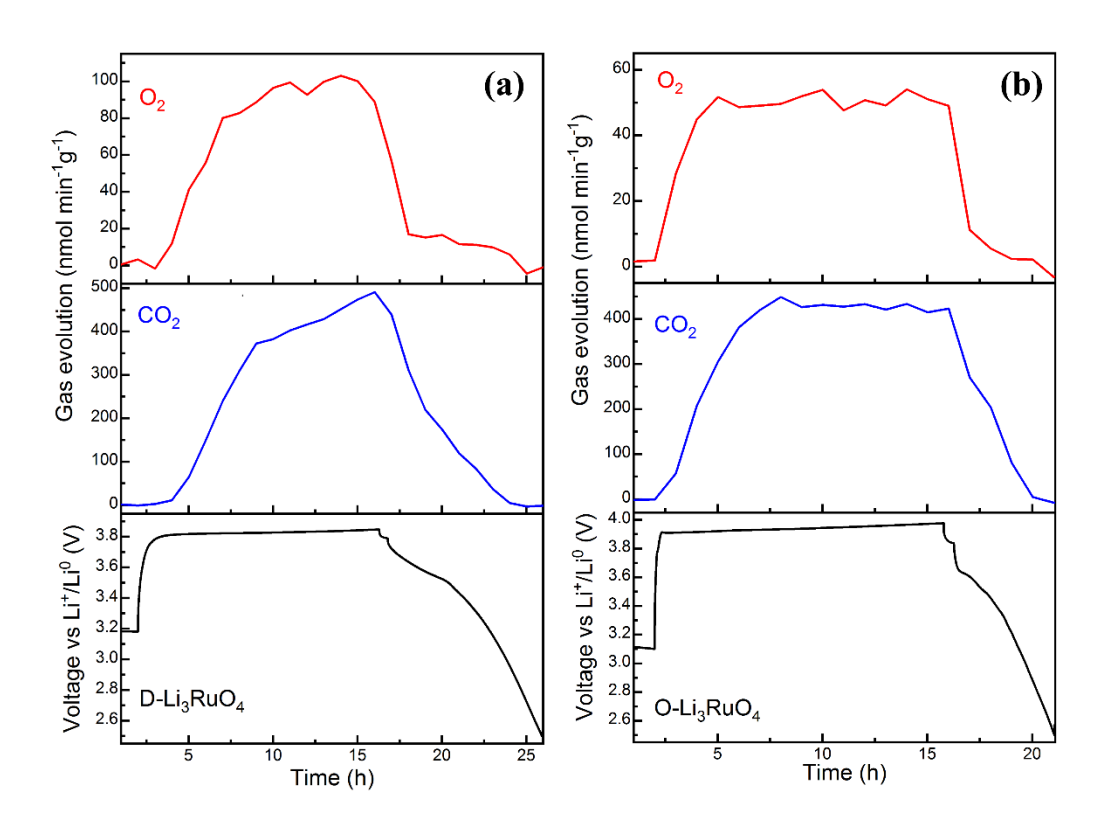


Figure 7. Operando gas evolution of D- (a) and O- (b) Li₃RuO₄, as measured by DEMS for the

first cycle.

2.3 Voltage cutoff window of 1.5-2.5 V

2.3.1 Electrochemical properties of Li₃RuO₄

D-Li₃RuO₄ between 1.5 and 2.5 V: When a cathodic current is applied onto pristine D-Li₃RuO₄, reduction was centered at 1.68 V vs Li⁺/Li⁰ (Figure 8a), accumulating charge equivalent to the intercalation of 0.8 mol Li per mol compound, consistent with the hypothetical reaction (2). A small step was further observed at 1.53 V. The profile of the following oxidation process showed a pseudo-plateau at 1.71 V, denoting a very small hysteresis, especially compared with the anodic process at high potential (Figure 1a and 1b). Approximately 0.7 mol Li was reversibly cycled at 2.5 V. The profiles remained almost the same upon subsequent redox cycles, with the exception of a subtle increase in the slope of the main pseudo-plateau (Figure 8a), manifested in an increased broadening of the associated peak in dQ/dV (Figure 8b), and the disappearance of any resolved signals below 1.55 V upon reduction. The amount of charge passed decreased only slightly with cycling (Figure S15), demonstrating a high reversibility of the redox process associated Li⁺ insertion/removal.

O-Li₃RuO₄ between 1.5 and 2.5 V: When the initial reduction was attempted on pristine O-Li₃RuO₄ (reaction (2)), a cathodic process proceeded via a long plateau around 1.72 V (Figure 8c), with the corresponding charge equivalent to the insertion of more than 1.6 mol Li per mol compound. The subsequent Li⁺ removal proceeded through two processes located at 1.8 and 1.89 V (Figure 8d), accounting for more than 1.3 mol Li. The electrochemical profile subtly evolved with cycling. In the second cycle, the cathodic profile shows two processes, at 1.74 and 1.7 V (Figure 8d), reversed at 1.8 and 1.9 V upon oxidation, denoting a greater hysteresis compared to

the disordered polymorph. With cycling, the two cathodic steps merged into a single pseudoplateau centered at 1.68 V (black arrow in Figure 8d). In contrast, two anodic processes remained, with an increase in slope (and width of the associated dQ/dV feature) and a slight shift toward lower potentials. The washing out of the profiles could be ascribed to an increased kinetic impediment to the reaction. The coulombic efficiency of each cycle was high (around 99.5%), but there was a progressive loss of capacity with cycling (Figure S16). The electrochemical signals in this low potential window were typical of conventional intercalation reactions in both polymorphs.

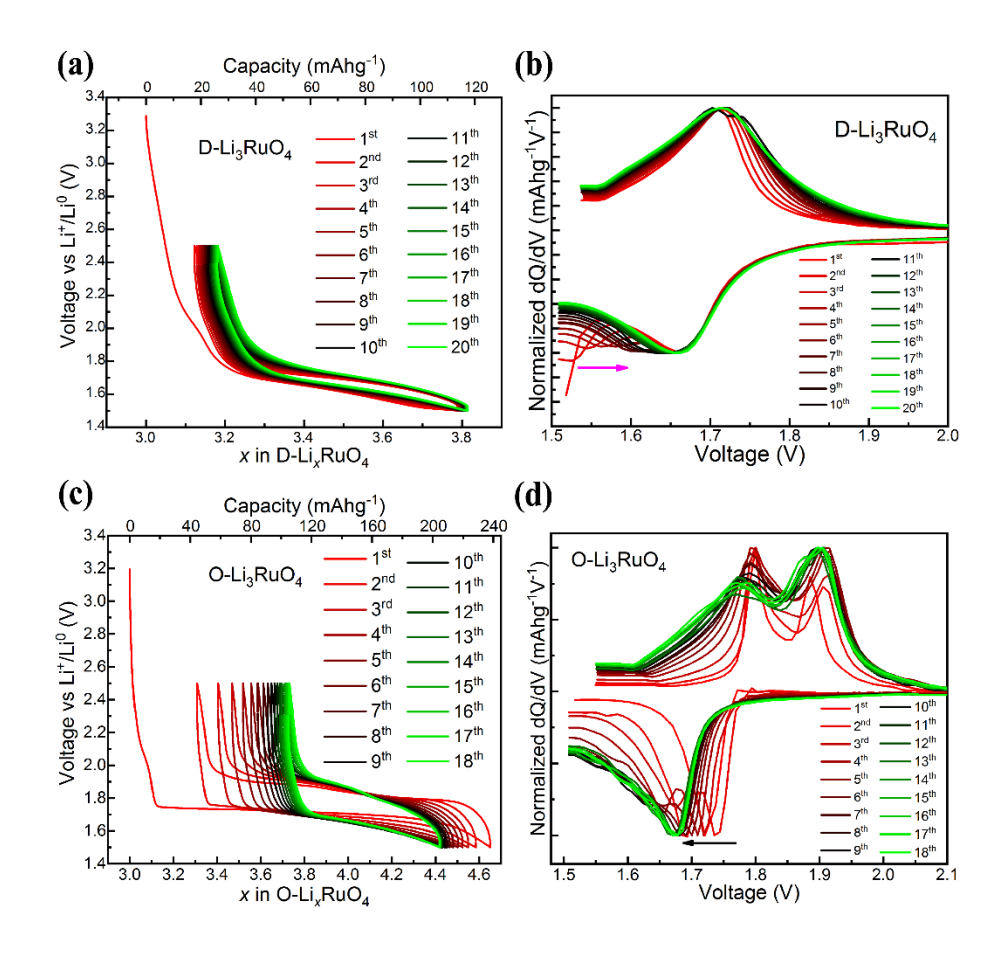


Figure 8. (a) Voltage-composition profile and the corresponding dQ/dV analysis of (a)-(b) D-Li₃RuO₄ and (c)-(d) O-Li₃RuO₄ between 1.5 and 2.5 V. The arrows denote the variations with cycling.

2.3.2 Structural variation of Li₃RuO₄

 $D\text{-}Li_3RuO_4$ between 1.5 and 2.5 V: The reduction of pristine D-Li_3RuO_4 to 1.5 V (reaction 2) gave rise to a pronounced shift of SXRD peak positions to lower angles, consistent with the insertion of Li⁺ into D-Li_3RuO_4, with no new reflections appearing, with the exception of a high angle tail in the most intense peak at Q = 3.3 Å⁻¹ (Figure 9). It also brought about peak broadening and intensity reduction in the *operando* SXRD patterns (Figure S17). The peak positions and intensity largely recovered via the following delithiation, indicating a reversible discharge and charge process. In comparison with the lattice size of the pristine state, Pawley refinements revealed that the reduction expanded the unit cell by 5.2% (Figure S18 and Table 2). The following oxidation shrank the unit cell, but with a slightly larger volume, by 0.32%, than the pristine state, indicating a small loss. Patterns collected at intermediate states during the *operando* measurement demonstrated a reversible solid solution process (Figure S17).

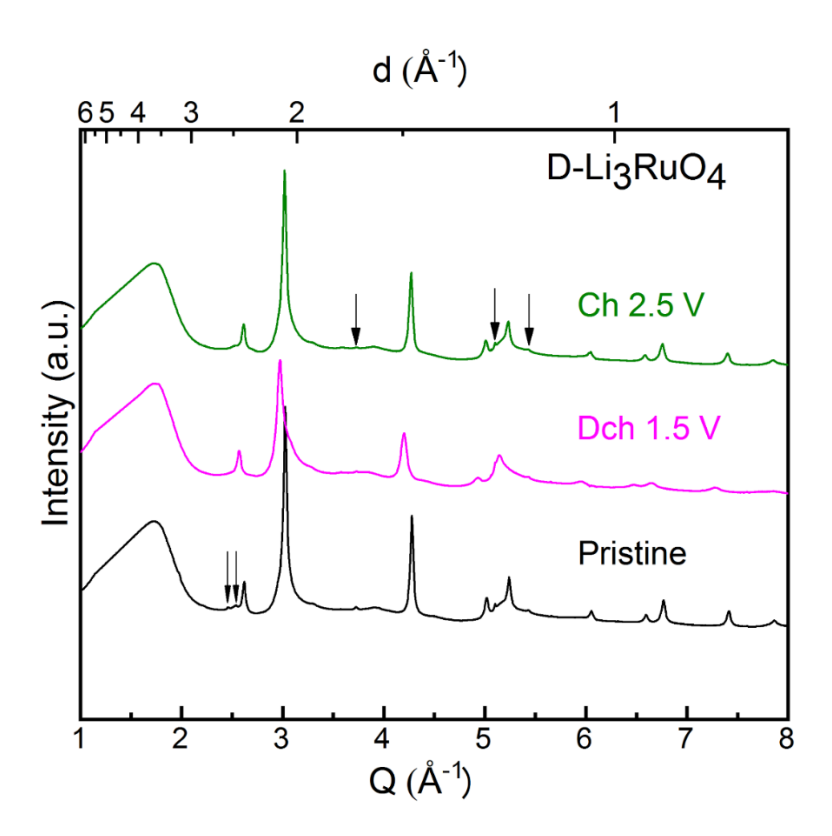


Figure 9. SXRD patterns of D-Li₃RuO₄ at selected points during the first cycle within a potential range of 1.5-2.5 V, collected *operando*. The complete evolution of the data is found in Figure S17. The black arrows denote the invariant Bragg reflections from the background only (Figure S19).

O-Li₃RuO₄ between 1.5 and 2.5 V: Reduction of pristine O-Li₃RuO₄ to 1.5 V (reaction 2) resulted in a shift of the diffraction peaks towards lower angles, concomitant to a decrease in their intensities (Figure 10). The final phase (Li_{4.6}RuO₄) was refined by the Rietveld refinement with a space group of P2/a, as in the pristine phase (Figure S20 and Table S4).²⁷ The unit cell size expanded by 18.0% in comparison with the pristine state after the reduction to 1.5 V (Table 2 and Figure S21), in good agreement with Jacquet *el al.*²⁷ The refinement was most satisfactory when electrochemically inserted Li⁺ ions were located in the tetrahedral sites of Li_{4.6}RuO₄, preserving ordering of Ru and Li in the metallic layer. In addition, there was a transition of the oxygen stacking from O3 type (ABCABC) to T1 type (ABAB) denoted by the large decrease in β angle

with respect to the pristine state.²⁷ After the following oxidation process, the structure recovered to the pristine state, except for an increase in peak widths, which is most likely ascribed to cycling-induced strain during the otherwise reversible transformation. The cycled product showed a smaller cell volume than the pristine state, by 6.9% (Table 2 and Figure S21). According to Jacquet *et al.*,²⁷ the peak splitting in dQ/dV plot upon oxidation, indicated by the discontinuity in the corresponding voltage-composition profile in the vicinity of x = 1.0, reflected a two-phase transition.⁴¹

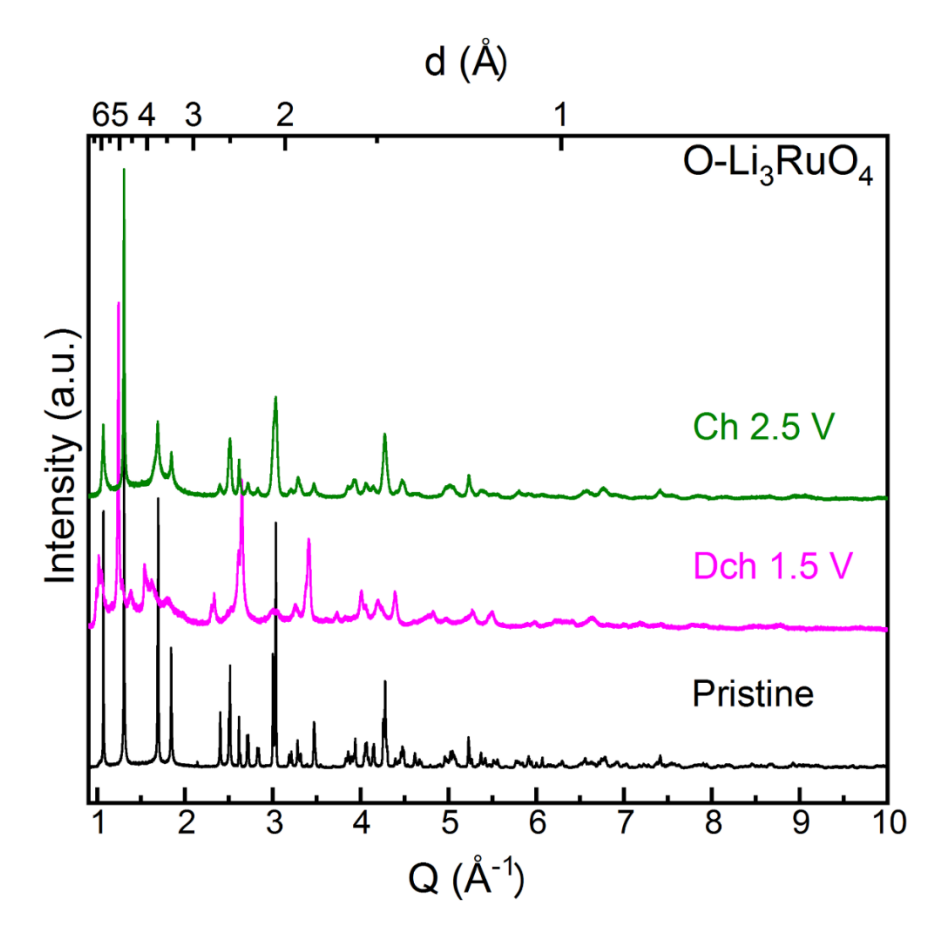


Figure 10. Ex situ SXRD patterns of O-Li₃RuO₄ at different electrochemical state within the range of 1.5-2.5 V.

Table 2 Calculated Unit Cell Parameters from SXRD patterns through Pawley refinement

D. I.; D., O.	
$D-Li_3RuO_4$	

State		a = b = c (Å)		Volume (Å ³)			
Pristine		4.14927	71.436				
Dch 1.5 V		4.22021	75.163				
Ch 2.5 V		4.15366	71.663				
O-Li ₃ RuO ₄							
State	a (Å)	b (Å)	c (Å)	β (°)	Volume (Å ³)		
Pristine	5.08809	5.86792	5.12213	110.154	143.566		
Dch 1.5 V	5.43544	6.16594	5.05606	90.6506	169.438		
Ch 2.5 V	5.07882	5.85193	5.10592	110.0275	142.574		

2.3.3 Ex situ Ru K-edge XAS of Li₃RuO₄

Reduction of D-Li₃RuO₄ to 1.5 V induced a pronounced shift of the absorption edge to lower energy by ~1.2 eV with respect to the pristine state, placing it close to RuO₂ (Figure 11a). The subsequent oxidation induced a shift of ~0.9 eV back toward high energy, with an almost completely reversible return to the pristine stae (Figure 11a). The shift of the absorption edge to lower energy upon reduction was larger for O-Li₃RuO₄ (~2.6 eV relative to the pristine state, Figure 12a). The final position was even lower than RuO₂ by around 0.6 eV, suggesting the final oxidation state of Ru was less than 4+, as could be expected from a capacity corresponding to 1.6 mol of inserted Li per formula unit. Upon oxidation to 2.5 V, the spectrum shifted back to higher energy, and almost superimposed with the pristine state (Figure 12a), clearly demonstrating the reversibility in electronic structure of Ru, in agreement with the observed electrochemical and structural changes.

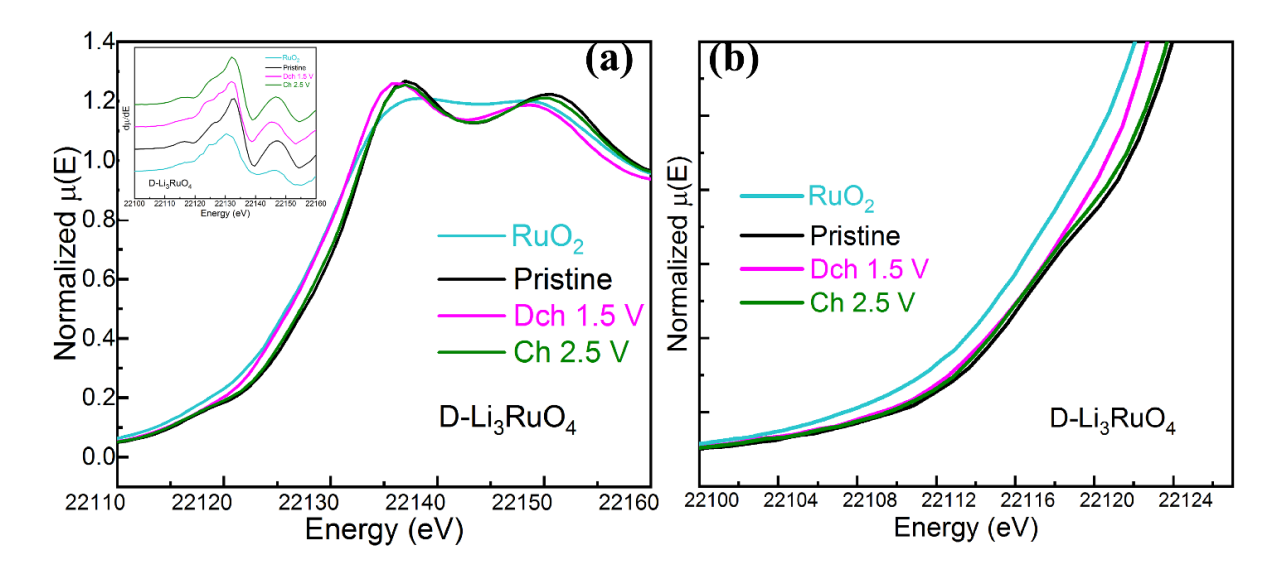


Figure 11. (a) *Ex situ* Ru K-edge XANES spectra of D-Li₃RuO₄ at different electrochemical states in the 1.5-2.5 V window, and (b) zoom of the pre-edge region. The inset in (a) presents the corresponding derivative curves, used to define the position of the absorption edge. RuO₂ was used as reference for Ru⁴⁺.

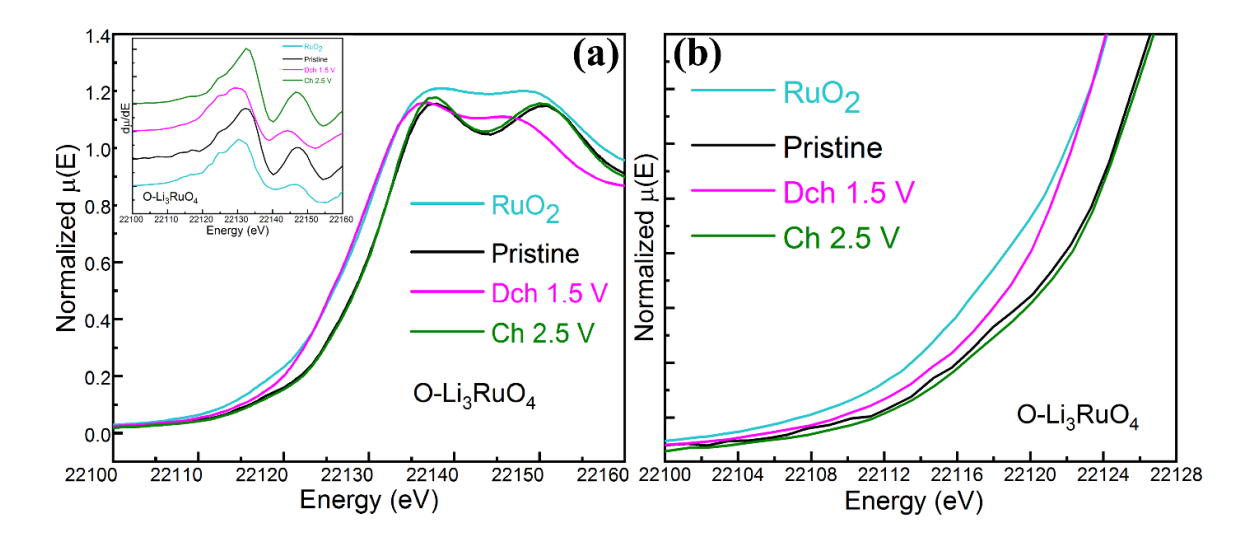


Figure 12. (a) *Ex situ* Ru K-edge XANES spectra of O-Li₃RuO₄ at different electrochemical states in the 1.5-2.5 V window, and (b) zoom of the pre-edge region. The inset in (a) presents the corresponding derivative curves, used to define the position of the absorption edge. RuO₂ was used as reference for Ru⁴⁺.

2.3.3 Ex situ O K-edge XAS of Li₃RuO₄

Li⁺ intercalation induced a shift of the O K-edge absorption threshold (jump above 535 eV) in both D- and O-Li₃RuO₄ to lower energy (Figures 13 and S22). The reduction led to a decrease in absorption intensity below 530 eV relative to the pristine state, especially at the lowest energies, leading to a broad feature dominated by a peak centered at 529.2 eV. The loss of intensity was more pronounced with the ordered polymorph, consistent with the higher measured capacity and degree of Ru reduction. The changes reflected the reversible occupation of state above the Fermi level during lithiation without severe reorganization of the O 2*p*-Ru 4*d* hybridization orbitals. The population of bands with a notable O character would reduce Z_{eff}, lowering the ionization threshold. The process was largely reversed upon oxidation in both compounds, indicating a high reversibility of the intercalation reaction.

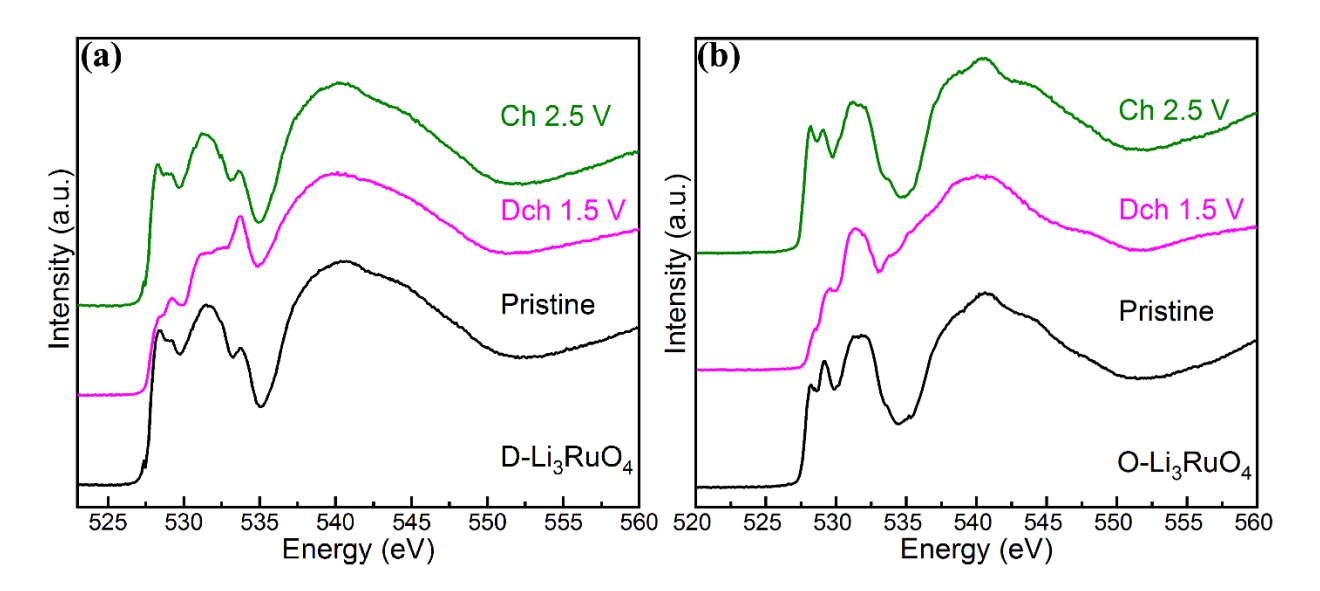
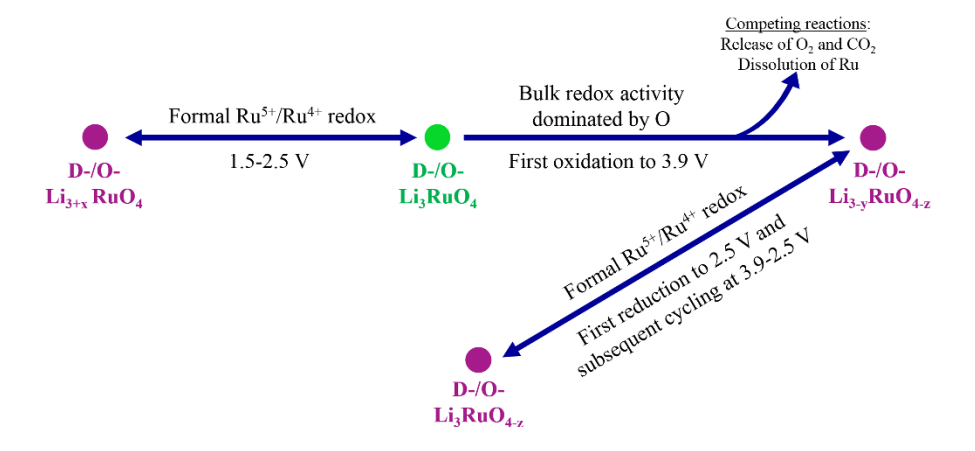


Figure 13. Ex situ O K-edge XAS spectra of (a) D- and (b) O-Li₃RuO₄ measured at different electrochemical states between 1.5 and 2.5 V.

3 Discussion

In this report, we comprehensively studied the intercalation chemistry of two Li₃RuO₄ polymorphs with a rock-salt framework to define charge compensation mechanisms at both metal and ligands. While some knowledge was available from O-Li₃RuO₄,^{27, 28} the comparison with D-Li₃RuO₄ enriches our understanding of the effect of crystallographic order, which is a design knob explored in recent research.⁴² Both compounds are capable of undergoing oxidation reactions above 3 V or reduction to 1.5 V from their pristine state, revealing a rich redox chemistry and varying degrees of reversibility. A visual summary is presented in Scheme 1.



Scheme 1. Summary of the electrochemical reactions of Li₃RuO₄ systems observed in this study.

Reactions within the 1.5-2.5 V window. We start discussing the electrochemical reaction observed in the voltage window of 1.5-2.5 V because of its simplicity. XAS results reveal in the electrochemical cell the induced reduction of Ru from an initial +5 to a final +4 formal state in the disordered polymorph, and even lower states for the ordered phase, as was also observed by Jacquet *et al.*^{27, 28} This behavior is accompanied by a commensurate decrease in the density of unoccupied states just above the Fermi level with an O 2*p*-Ru 4*d* contribution. Therefore, both Ru

and O contribute to the states that accommodate the injected electrons. The fact that no new states were observed in the O 2*p*-Ru 4*d* states indicates similar Ru-O interactions, with perhaps the exception of a slight decrease in covalency of the bond. This observation is supported by the topotactic change in crystal structure and the absence of obvious deviations from an octahedral coordination of Ru.²⁸ The reaction was chemically reversible, with the compound returning close to the pristine state upon re-oxidation, and energy efficient, measured by a combined high coulombic efficiency and low hysteresis in potential. All these characteristics correspond to a conventional mechanism of interaction of lithium (Scheme 1):⁴³

$$\text{Li}_3\text{Ru}^{5+}\text{O}^{2-}_4 + x\text{Li}^+ + x\text{e}^- \leftrightarrow \text{Li}_{3+x}\text{Ru}^{(5-x)+}\text{O}^{2-}_4$$
 (3)

where charge compensation is assigned based on the changes in the formal oxidation state of the metal as proxy for states with participation of both metal and O due to the high covalency of these compounds. There were only slight differences in the reversibility of the two polymorphs, with the disordered polymorph showing lower losses in capacity upon many cycles. This disparate behavior likely stems from the different reaction mechanisms: solid solution for D-Li₃RuO₄, and as reported by Jacquet *et al.* multiphasic for O-Li₃RuO₄.²⁷ These different mechanisms will also lead to differences in kinetic barriers to the transformation, providing an explanation to the different degrees of hysteresis in potential, likely due to polarization.

Reactions during the first oxidation to 3.9 V. During this first oxidation, the reactions were not conventional, yet fundamentally the same in both polymorphs. The measured capacities were large, especially in D-Li₃RuO₄, in a faradaic process that changed the bulk structure of the oxide in a seemingly topotactic manner, consistent with Li deintercalation, according to XRD (Figures 2 and 3a). The increase in the unit cell volume may be due to the increased electrostatic repulsion between transition metal clusters that are less screened because of the Li⁺ removal. Yet only small

apparent changes were observed by XAS in the electronic state of Ru in the oxidized phase (Figure 4 and 5), especially in comparison with the notable reorganization of the O 2*p*-Ru 4*d* states probed by the pre-edge features in the O K-edge spectra (Figure 6). Furthermore, the position of the absorption edge of O subtly shifted to higher energies, indicative of a greater Z_{eff}. ^{35, 44} Therefore, Li deintercalation was accompanied by changes in electronic structure of the solid oxide that heavily involved changes at the O ligands, including depletion of their charge.

The overall oxidation process also involved the evolution of O₂ and CO₂ at the onset of the oxidation in our experiments (Figure 7), possibly indicating the robust surface activity. The fact that spectral signals associated with Li₂CO₃ persisted throughout oxidation (Figures S12 and S13) suggests that CO₂ does not primarily arise from decomposition of these solid impurities, consistent with observations of its redox potential in the literature.³⁸ Recently, an interfacial mechanism was proposed by Jacquet *et al.* whereby Ru ions could be oxidized and then partially dissolved, after removing Li from O-Li₃RuO₄, in the form of soluble RuO₄ and RuO₄⁻¹ species, leading to black coloring, which could react with the electrolyte and release CO₂.²⁸ This mechanism could also explain the observation of black discoloration on the surface of the separator after charging O-Li₃RuO₄ to 3.9 V (Figure S23), despite the relatively small capacity compared to the disordered polymorph. However, soluble RuO₄ and RuO₄⁻¹ species should not be detectable in our XAS experiments, which were collected on washed solid electrodes, especially considering the detection modes used in all cases.

Taking all these facts together, the following reaction could be postulated (Scheme 1):

$$\text{Li}_3\text{RuO}_4 \rightarrow \text{Li}_{3-y}\text{RuO}_{4-z} + y\text{Li}^+ + x\text{e}^- + (z/2)\text{O}_2$$
 (4)

where y = x + 2z, reflecting both the loss of O from the lattice ($z \sim 0.05$ -0.1 based solely on the evolution of O_2) and the charge compensation at lattice O. Formal charges are challenging to

ascribe, since both Ru and O underwent spectroscopic changes, albeit much more pronounced in the latter case. Indeed, XAS clearly points at a strong increase in the contribution of O to states above the Fermi level from Li₃RuO₄ to Li_{3-y}RuO_{4-z}. While the RuO₆ octahedron is reported to distort during the first oxidation, no structural evidence is available of the existence of O-O interactions,²⁸ which is primarily a structural feature that cannot be probed by XAS unless other information is available.⁴⁵

This reaction competes with deleterious Ru dissolution and electrolyte decomposition. Dissolution is not constant during charging, instead depending on the actual amount of electrons extracted from the material. Using data provided by Jacquet *et al.*,²⁸ we estimate that the oxidation of O-Li₃RuO₄ in our conditions (Figure 1) led to less than 5% loss of mass because the capacity never exceeded the equivalent of 1 mol Li per mol oxide. In contrast, the capacity D-Li₃RuO₄ was equivalent to ~1.9 mol Li per mol oxide. No data on dissolution is available for this polymorph, but it is reasonable to assume that the trends for O-Li₃RuO₄ reported by Jacquet *et al.* are a good approximation. At this level of oxidation their data would predict a ~15-20% loss of mass of the active material, which would account for to 0.375-0.5 mol electrons out of a total of ~1.9 mol electrons extracted. All in all, the data from Jacquet *et al.* support that the bulk process is dominant in our experiments.

Reactions during the first reduction from 3.9 V to 2.5 V, and subsequent cycling. The existence of irreversible interfacial reactions contributed to the coulombic inefficiency observed in the first oxidation-reduction cycle of both polymorphs. Nonetheless, there was significant electrochemical and structural activity above 2.5 V upon subsequent reduction. Since pristine Li₃RuO₄ would not intercalate Li at these potentials (vide supra), this behavior further confirms the deintercalation of Li upon oxidation. Consistent with an intercalation reaction, the rock-salt structure was found to

shrink back toward the initial volume. However, this reaction did not restore either the Ru K-edge or O K-edge XAS spectrum for the pristine state. Indeed, clear reduction of formal Ru⁵⁺ to Ru⁴⁺ occurred, as indicated by the shift of the Ru K-edge. If the electrode was discharged all the way to 1.5 V, the Ru K-edge appeared at even lower energies than Li_{3+x}RuO₄ formed directly via reaction 3 (Figures S24 and S25).

The different pathway of changes in electronic state during oxidation-reduction are consistent with the large hysteresis in the electrochemical profile of the first cycle. Although no specific analysis was made, we observed that measurements of Ru by Jacquet *et al.* also revealed different pathways during the first cycle, ²⁸ where equal electrode capacities led to notably greater Ru participation during reduction than oxidation. The prominent decrease in the population of unoccupied O 2*p*-Ru 4*d* states in O K-edge XAS, especially at the lowest energies, would also be in good agreement with the Ru⁵⁺/Ru⁴⁺ formal redox couple. This conclusion is reinforced by the comparison of both the Ru K-edge and the pre-edge part in the O K-edge TFY spectrum between the first reduction from 3.9 to 2.5 V and the initial reduction from pristine to 1.5 V, which revealed a strong similarity in the spectra (Figures S26, S27 and S28), suggesting similar electronic changes in both cases. However, it is important to emphasize that the crystal structure of these two reduced state is different, as can be most clearly seen for the ordered polymorph by comparing "Dch 2.5 V Max Cap" in Figure 3 with "Dch 1.5 V" in Figure 10. Therefore, overall, the reactions happening are different in both potential ranges.

The changes at both O and Ru in O-Li₃RuO₄ during the first discharge were very similar with the cycle at which the highest electrochemical activity was achieved. In other words, while the first oxidation was chemically irreversible, subsequent cycling proceeded through the same Ru-O couples. Therefore, the following mechanism is postulated to operate upon the first reduction to

2.5 V (Scheme 1):

$$\text{Li}_{3-y}\text{RuO}_{4-z} + y\text{Li}^+ + y\text{e}^- \leftrightarrow \text{Li}_3\text{RuO}_{4-z}$$
 (5)

This mechanism corresponds to a conventional intercalation reaction centered on the formal state of the transition metal, which again, in reality, reflects the covalence of the Ru-O bond. It is important to note that this change in mechanism was accompanied by a significant decrease in hysteresis of the voltage profile, to a degree reminiscent of conventional intercalation reactions. Indeed, the changes in the XRD patterns of O-Li₃RuO₄ were more pronounced upon activation than in the first cycle, but they appeared topotactic in nature. This behavior is ascribed to a progressive activation of a larger portion of the electrode as cycling proceeded, indicating that the first oxidation was limited by sluggish kinetics. The much smaller O₂ release in the second cycle, compared with the first is in agreement with both the proposed mechanism and the progressive activation of pristine domains upon cycling (Figure S29 and Table S3).

Upon extensive cycling, both polymorphs displayed a quite different trend in performance, with a continuous for D-Li₃RuO₄ (Figure S5), compared to a sustained electrochemical activation for O-Li₃RuO₄ until its highest electrochemical reactivity was equivalent to the cycling of 1 mol Li per mol Li₃RuO₄ (Figure S6). The faradaic yields are expected to be high at this point in the reaction, since XAS reveals cycling between Ru⁵⁺ and Ru⁴⁺, a 1 e⁻ process. In comparison with the report by Jacquet *et al.* that oxidation of O-Li₃RuO₄ to 4.2 V could remove around 3 mol Li, but led to an irreversible change in the lattice,²⁷ the solution was to limit the voltage (decrease the capacity) to impart stability. The large removal of Li from D-Li₃RuO₄ upon the first oxidation to the same potential as O-Li₃RuO₄ could be an indication of better kinetics due to the enhanced diffusion due to improved percolation of active Li diffusion channels in a disordered rock-salt.⁴² Possibly, the very high capacity reached for D-Li₃RuO₄ in the first cycle was detrimental to its

cycling stability because more dissolution of Ru would be expected at these levels of oxidation. Indeed, experiments where the first charge capacity was limited yielded a similar evolution in voltage profile as O-Li₃RuO₄, with an increase in cycling stability (Figure S30).

It is striking that the same formal redox couple (Ru⁵⁺/Ru⁴⁺) could be accessed at two very different potentials, 3.7-3.8 V vs. ~1.8 V. The difference appears to be rooted in the role of crystal structure in defining the chemical potential of Li in each structure, Li₃RuO₄₋₂ vs. Li_{3+x}Ru^{(5-x)+}O²⁻4, respectively. Whereas Li would be expected to (de)intercalate (from) into octahedral sites in the former, the excess of Li (x) in the latter stuffs the rock-salt framework, leading to the introduction of Li in tetrahedral sites. The different relative location of cations in the structure in both cases is hypothesized to be a stronger driver than the formal redox couple in this system. This behavior is reminiscent of LiMn₂O₄, a classical battery material with a spinel structure. It undergoes removal of Li from tetrahedral sites at ~4 V to form Mn₂O₄, whereas insertion of Li at 2.9 V displaces all alkali metal cations to octahedral sites to form Li₂Mn₂O₄.⁴⁶ The formal Mn³⁺/Mn⁴⁺ couple is involved in both cases, but it is worth noting the smaller difference in potential (1.1 V) compared to Li₃RuO₄ here (~2 V), and the fact that the metal centers involved in each process are nominally different, as the initial material contains both Mn³⁺ and Mn⁴⁺.

4 Conclusion

Two rock-salt polymorphs of Li₃RuO₄ were successfully synthesized with disordered and ordered Li/Ru arrangements. Synchrotron diffraction and X-ray absorption spectroscopy were employed to define the changes in crystal and electronic structure when Li was cycled from the structure. Between 1.5 and 2.5 V, both polymorphs undergo a conventional, reversible reaction of Li intercalation compensated by the formal Ru⁵⁺-Ru⁴⁺ couple via O 2*p*-Ru 4*d* hybridization.

Greater reversibility and stability was observed for the disordered compound due to its solidsolution mechanism. When Li₃RuO₄ is oxidized to 3.9 V instead, charge compensation follows an unconventional mechanism with much more noticeable changes in the O than Ru states, accompanied by competing irreversible, yet minor O₂ loss and Ru dissolution. When this oxidized state is reduced to 2.5 V and subsequently cycled, a reversible topotactic intercalation takes place, with the charge compensation following a conventional redox process through the formal Ru⁵⁺-Ru⁴⁺ couple. This process reduces irreversibility compared to the first charge, leading to stable cycling, especially in the ordered polymorph. Overall, the combined study comprehensively demonstrates the complex intercalation chemistry of Li₃RuO₄ and the significance of the Ru-O covalency in compensating the associated electrochemical changes. This compound can access the formal Ru⁵⁺-Ru⁴⁺ couple at two very different potentials, an unusual occurrence in solid state chemistry. In turn, the chemical irreversibility (but reversible capacity) of the reaction of Li deintercalation to 3.9 V, to directly access O states, highlights the challenge of efficiently using this reactivity in an electrochemical device without capacity loss or hysteresis. This fundamental study offers new light into our ability to tap the chemical bond in solids to conduct electrochemical reactions that have significance to energy storage with high energy density.

ASSOCIATED CONTENT

Supporting Information

Experimental details, Figures S1-S30 and Tables S1-S4

Acknowledgements

This material is entirely based upon work supported by the National Science Foundation under Grant No. DMR-1809372. All synchrotron measurements used resources of the Advanced Photon Source, a U.S. Department of Energy (DOE) Office of Science User Facility operated for the DOE Office of Science by Argonne National Laboratory under Contract No. DE-AC02-06CH11357. The authors thank Zhengyan Lun, from the University of California-Berkeley, for support with XAS measurements.

Bibliography

- 1. Noorden, R. V., The rechargeable revolution: A better battery. *Nature* **2014**, 507, 26-28.
- 2. Whittingham, M. S., Lithium Batteries and Cathode Materials. *Chem. Review.* **2004**, 104, 4271-4302.
- 3. Dunn, B.; Kamath, H.; Tarascon, J.-M., Electrical Energy Storage for the Grid: A Battery of Choices. *Science* **2011**, 334, 928-935.
- 4. Larcher, D.; Tarascon, J. M., Towards greener and more sustainable batteries for electrical energy storage. *Nat. Chem.* **2015,** *7,* 19-29.
- 5. Armand, M.; Tarascon, J. M., Building better batteries. *Nature* **2008**, 451, 652-657.
- 6. Goodenough, J. B.; Kim, Y., Challenges for Rechargeable Li Batteries†. *Chem. Mater.* **2010,** 22, 587-603.
- 7. Ellis, B. L.; Lee, K. T.; Nazar, L. F., Positive Electrode Materials for Li-Ion and Li-Batteries†. *Chem. Mater.* **2010**, 22, 691-714.
- 8. Mizushima, K.; Jones, P. C.; Wiseman, P. J.; Goodenough, J. B., Li_xCoO₂ (0<x<-1): A new cathode material for batteries of high energy density. *Mater. Res. Bull.* **1980**, 15, 783-789.

- 9. Lu, Z.; MacNeil, D. D.; Dahn, J. R., Layered Li[Ni_xCo_{1-2x}Mn_x]O₂ Cathode Materials for Lithium-Ion Batteries. *Electrochem. Solid-State Lett.* **2001**, 4, A200-A203.
- 10. Yabuuchi, N.; Ohzuku, T., Novel lithium insertion material of LiCo_{1/3}Ni_{1/3}Mn_{1/3}O₂ for advanced lithium-ion batteries. *J. Power Sources* **2003**, 119-121, 171-174.
- 11. Lu, Z.; MacNeil, D. D.; Dahn, J. R., Layered Cathode Materials Li[Ni_xLi_(1/3-2x/3)Mn_(2/3-x/3)]O₂ for Lithium-Ion Batteries. *Electrochem. Solid-State Lett.* **2001,** 4, A191-A194.
- 12. Johnson, C. S.; Kim, J. S.; Lefief, C.; Li, N.; Vaughey, J. T.; Thackeray, M. M., The significance of the Li₂MnO₃ component in 'composite' xLi₂MnO₃·(1–x)LiMn_{0.5}Ni_{0.5}O₂ electrodes. *Electrochem. Commun.* **2004**, 6, 1085-1091.
- 13. Rozier, P.; Tarascon, J. M., Review—Li-Rich Layered Oxide Cathodes for Next-Generation Li-Ion Batteries: Chances and Challenges. *J. Electrochem. Soc.* **2015**, 162, A2490-A2499.
- 14. Thackeray, M. M.; Kang, S.-H.; Johnson, C. S.; Vaughey, J. T.; Benedek, R.; Hackney, S. A., Li₂MnO₃-stabilized LiMO₂ (M = Mn, Ni, Co) electrodes for lithium-ion batteries. *J. Mater. Chem.* **2007**, 17, 3112-3125.
- 15. Luo, K.; Roberts, M. R.; Hao, R.; Guerrini, N.; Pickup, D. M.; Liu, Y. S.; Edstrom, K.; Guo, J.; Chadwick, A. V.; Duda, L. C.; Bruce, P. G., Charge-compensation in 3d-transition-metal-oxide intercalation cathodes through the generation of localized electron holes on oxygen *Nat. Chem.* **2016**, 8, 684-91.
- 16. Sathiya, M.; Rousse, G.; Ramesha, K.; Laisa, C. P.; Vezin, H.; Sougrati, M. T.; Doublet, M. L.; Foix, D.; Gonbeau, D.; Walker, W.; Prakash, A. S.; Ben Hassine, M.; Dupont, L.; Tarascon,

- J. M., Reversible anionic redox chemistry in high-capacity layered-oxide electrodes. *Nat. Mater.* **2013**, 12, (9), 827-35.
- 17. Lee, J.; Seo, D.-H.; Balasubramanian, M.; Twu, N.; Li, X.; Ceder, G., A new class of high capacity cation-disordered oxides for rechargeable lithium batteries: Li–Ni–Ti–Mo oxides. *Energy Environ. Sci.* **2015**, 8, 3255-3265.
- 18. Wang, R.; Li, X.; Liu, L.; Lee, J.; Seo, D.-H.; Bo, S.-H.; Urban, A.; Ceder, G., A disordered rock-salt Li-excess cathode material with high capacity and substantial oxygen redox activity: Li_{1.25}Nb_{0.25}Mn_{0.5}O₂. *Electrochem. Commun.* **2015**, 60, 70-73.
- 19. Yabuuchi, N.; Takeuchi, M.; Nakayama, M.; Shiiba, H.; Ogawa, M.; Nakayama, K.; Ohta, T.; Endo, D.; Ozaki, T.; Inamasu, T.; Sato, K.; Komaba, S., High-capacity electrode materials for rechargeable lithium batteries: Li₃NbO₄-based system with cation-disordered rocksalt structure. *Proc. Natl. Acad. Sci.* **2015**, 112, 7650-7655.
- 20. Kan, W. H.; Chen, D.; Papp, J. K.; Shukla, A. K.; Huq, A.; Brown, C. M.; McCloskey, B. D.; Chen, G., Unravelling Solid-State Redox Chemistry in Li_{1.3}Nb_{0.3}Mn_{0.4}O₂ Single-Crystal Cathode Material. *Chem. Mater.* **2018**, 30, 1655-1666.
- 21. Freire, M.; Kosova, N. V.; Jordy, C.; Chateigner, D.; Lebedev, O. I.; Maignan, A.; Pralong, V., A new active Li-Mn-O compound for high energy density Li-ion batteries. *Nat. Mater.* **2016,** 15, 173-7.
- 22. Pearce, P. E.; Perez, A. J.; Rousse, G.; Saubanere, M.; Batuk, D.; Foix, D.; McCalla, E.; Abakumov, A. M.; Van Tendeloo, G.; Doublet, M. L.; Tarascon, J. M., Evidence for anionic redox activity in a tridimensional-ordered Li-rich positive electrode beta-Li₂IrO₃. *Nat. Mater.* **2017**, 16, 580-586.

- 23. Seo, D. H.; Lee, J.; Urban, A.; Malik, R.; Kang, S.; Ceder, G., The structural and chemical origin of the oxygen redox activity in layered and cation-disordered Li-excess cathode materials. *Nat. Chem.* **2016**, 8, 692-7.
- 24. Saubanère, M.; McCalla, E.; Tarascon, J. M.; Doublet, M. L., The intriguing question of anionic redox in high-energy density cathodes for Li-ion batteries. *Energy Environ. Sci.* **2016**, 9, 984-991.
- 25. Xie, Y.; Saubanère, M.; Doublet, M. L., Requirements for reversible extra-capacity in Lirich layered oxides for Li-ion batteries. *Energy Environ. Sci.* **2017**, 10, (1), 266-274.
- 26. Perez, A. J.; Jacquet, Q.; Batuk, D.; Iadecola, A.; Saubanère, M.; Rousse, G.; Larcher, D.; Vezin, H.; Doublet, M.-L.; Tarascon, J.-M., Approaching the limits of cationic and anionic electrochemical activity with the Li-rich layered rocksalt Li₃IrO₄. *Nat. Energy* **2017**, 2, 954-962.
- 27. Jacquet, Q.; Perez, A.; Batuk, D.; Van Tendeloo, G.; Rousse, G.; Tarascon, J.-M The $\text{Li}_3\text{Ru}_y\text{Nb}_{1-y}\text{O4}$ ($0 \le y \le 1$) System: Structural Diversity and Li Insertion and Extraction Capabilities. *Chem. Mater.* **2017**, 29, 5331-5343.
- 28. Jacquet, Q.; Iadecola, A.; Saubanère, M.; Lemarquis, L.; Berg, E. J.; Alves Dalla Corte, D.; Rousse, G.; Doublet, M.-L.; Tarascon, J.-M., Competition between Metal Dissolution and Gas Release in Li-Rich Li₃Ru_yIr_{1-y}O₄ Model Compounds Showing Anionic Redox. *Chem. Mater.* **2018**, 30, 7682-7690.
- 29. Soma, M.; Sato, H., Lithium Ruthenates: Controlling Dimensionality and Topology of Magnetic-Ion Arrangements. *J. Phy. Soc. Jpn* **2006**, 75, 124802.
- 30. Jacquet, Q.; Rousse, G.; Iadecola, A.; Saubanère, M.; Doublet, M.-L.; Tarascon, J.-M., Electrostatic Interactions versus Second Order Jahn–Teller Distortion as the Source of Structural Diversity in Li₃MO₄ Compounds (M = Ru, Nb, Sb and Ta). *Chem. Mater.* **2018**, 30, 392-402.

- 31. Alexander, A.; Battle, P. D.; Burley, J. C.; Gallon, D. J.; Grey, C. P.; Kim, S. H., Structural and magnetic properties of Li₃RuO₄. *J. Mater. Chem.* **2003**, 13, 2612.
- 32. Bush, T. S.; Catlow, C. R. A.; Battle, P. D., Evolutionary programming techniques for predicting inorganic crystal structures. *J. Mater. Chem.* **1995**, 5, 1269-1272.
- 33. Yamamoto, T., Assignment of pre-edge peaks in K-edge x-ray absorption spectra of 3d transition metal compounds: electric dipole or quadrupole? *X-Ray Spectrom.* **2008,** 37, 572-584.
- 34. dE Groot, F.; Kotani, A., Core Level Spectroscopy of Solids; Advances in Condensed Matter Science (CRC Press, 2008) 2008.
- 35. Shadle, S. E.; Hedman, B.; Hodgson, K. O.; Solomon, E. I., Ligand K-Edge X-ray Absorption Spectroscopy as a Probe of Ligand-Metal Bonding: Charge Donation and Covalency in Copper-Chloride Systems. *Inorg. Chem.* **1994**, 33, 4235-4244.
- 36. Wasinger, E. C.; de Groot, F. M. F.; Hedman, B.; Hodgson, K. O.; Solomon, E. I., L-edge X-ray Absorption Spectroscopy of Non-Heme Iron Sites: Experimental Determination of Differential Orbital Covalency. *J. Am. Chem. Soc.* **2003**, 125, 12894-12906.
- 37. Qiao, R.; Chuang, Y. D.; Yan, S.; Yang, W., Soft x-ray irradiation effects of Li₂O₂, Li₂CO₃ and Li₂O revealed by absorption spectroscopy. *PLoS One* **2012**, 7, e49182.
- 38. Ling, C.; Zhang, R.; Takechi, K.; Mizuno, F., Intrinsic Barrier to Electrochemically Decompose Li₂CO₃ and LiOH. *J. Phys. Chem. C* **2014**, 118, 26591-26598.
- 39. Mahne, N.; Renfrew, S. E.; McCloskey, B. D.; Freunberger, S. A., Electrochemical Oxidation of Lithium Carbonate Generates Singlet Oxygen. *Angew. Chem. Int. Ed.* **2018**, 57, 5529-5533.

- 40. Renfrew, S. E.; McCloskey, B. D., Residual Lithium Carbonate Predominantly Accounts for First Cycle CO₂ and CO Outgassing of Li-Stoichiometric and Li-Rich Layered Transition-Metal Oxides. *J. Am. Chem. Soc.* **2017**, 139, 17853-17860.
- 41. Moreau, P.; Guyomard, D.; Gaubicher, J.; Boucher, F., Structure and Stability of Sodium Intercalated Phases in Olivine FePO₄. *Chem. Mater.* **2010**, 22, 4126-4128.
- 42. Lee, J.; Urban, A.; Li, X.; Su, D.; Hautier, G.; Ceder, G., Unlocking the Potential of Cation-Disordered Oxides for Rechargeable Lithium Batteries. *Science* **2014**, 343, 519-522.
- 43. Whittingham, M. S., Ultimate Limits to Intercalation Reactions for Lithium Batteries. *Chem. Rev.* **2014**, 114, 11414-11443.
- 44. Shadle, S. E.; Hedman, B.; Hodgson, K. O.; Solomon, E. I., Ligand K-edge x-ray absorption spectroscopic studies: metal-ligand covalency in a series of transition metal tetrachlorides. *J. Am. Chem. Soc.* **1995**, 117, 2259-2272.
- 45. Grimaud, A.; Iadecola, A.; Batuk, D.; Saubanère, M.; Abakumov, A. M.; Freeland, J. W.; Cabana, J.; Li, H.; Doublet, M.-L.; Rousse, G.; Tarascon, J.-M., Chemical Activity of the Peroxide/Oxide Redox Couple: Case Study of Ba₅Ru₂O₁₁ in Aqueous and Organic Solvents. *Chem. Mater.* **2018**, 30, 3882-3893.
- 46. Ohzuku, T., Electrochemistry of Manganese Dioxide in Lithium Nonaqueous Cell. *J. Electrochem. Soc.* **1990,** 137, 769.

For Table of Contents Use Only

Definition of Redox Centers in Reactions of Lithium Intercalation in Li₃RuO₄ Polymorphs

Haifeng Li,[†] Srinivasan Ramakrishnan,[‡] John W. Freeland,[§] Bryan D. McCloskey,[‡] Jordi Cabana*,[†]

[†]Department of Chemistry, University of Illinois at Chicago, Chicago, Illinois 60607, United States

[‡]Department of Chemical and Biomolecular Engineering, University of California, Berkeley, California 94720, United States

§Advanced Photon Source, Argonne National Laboratory, Lemont, Illinois 60439, United States

